A Flexible Lightweight 7.4 V Input 300 V to 1500 V Output Power Converter for an Untethered Modular Piezoelectric Soft Robot

Hsin Cheng, Zhiwu Zheng, Prakhar Kumar, Yenan Chen, Jaeil Baek,
Ben Kim, Sigurd Wagner, Naveen Verma, James C. Sturm, and Minjie Chen
Princeton University, Princeton, NJ, USA
Email: {hsin, zhiwuz, minjie}@princeton.edu

2023 IEEE 24th Workshop on Control and Modeling for Power Electronics (COMPEL) | 979-8-3503-1618-6/23/$31.00 ©2023 IEEE | DOI: 10.1109/COMPEL52896.2023.10221022

***Abstract*—Soft robot is an enabling technology for many emerging applications. The operation voltages of many electric soft actuators, i.e., Macro Fiber Composites (MFC) and Dielectric Elastomer Actuators (DEA), are usually in the range of hundreds to thousands of volts. Actuators in a soft robot often need to be coordinated efficiently, precisely or rapidly, to perform useful functions such as crawling, jumping, or swimming. This paper presents the design and implementation of a flexible, lightweight, and modular power converter for multi-actuator piezoelectric soft robots. Output pulses of 300 V to 1500 V, 1 W, can be generated from 7.4 V input voltage with less than 5 g of power electronics weight. A fully untethered, modular, scalable soft robot platform enables new opportunities for hardware, software, power, and control co-design.**

***Index Terms*—soft robots, piezoelectric actuators, high voltage, DC-DC, switched-capacitor, diode multiplier.**

I. Introduction

Untethered soft robots require flexible, lightweight, and efficient power electronics. Piezoelectric actuators are widely utilized for soft robotic actuation [1]–[4] because of their high scalability, control precision, and power density [5]. They are also compatible with large-area electronics manufacturing processes. Piezoelectric actuators usually require hundreds or even above a thousand volts, while only low-voltage batteries ($<$10 V) are available as energy sources for an untethered soft robot. Additionally, for a multi-actuator soft robot, scalability of the power electronics is important because the actuators need to be excited independently to achieve complex locomotion. Therefore, a lightweight, modular, and scalable power architecture that can efficiently control a group of high-voltage piezoelectric actuators from low-voltage energy sources is needed. It is the principal focus of this paper.

Existing high voltage power electronics can be grouped into two main categories: (1) transformer-based [6]–[11]; and (2) transformer-less [12]–[14]. In transformer-based design, the circuit usually consists of an inverter, a transformer, and a voltage rectifier or multiplier. The required voltage gain is contributed by many stages. In a transformer-less architecture, the circuits are composed of a variation of boost converters and a voltage rectifier or multiplier stage. Switched-capacitor circuits are also attractive [13], [14]. We adopt a transformer-based design, because (1) transformers can offer high conversion ratios with very light weight ($\sim$0.5 g), ideal for high-voltage, lightweight power converters; (2) this design helps to reduce the switch stress and thus the package size of switches; and (3) it has the potential to achieve high efficiency. The proposed hybrid switched-capacitor-transformer architecture combines the advantages of transformers and capacitive voltage multipliers.

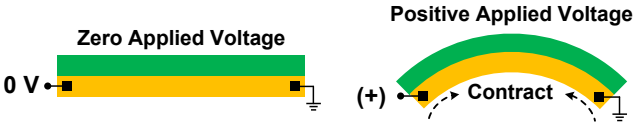

Fig. 1. The operation of a piezoelectric actuator bonded to a steel foil. The yellow layer represents the piezoelectric actuator, and the green layer stands for the steel foil. When a positive voltage is applied, the actuator-steel structure bends concave down.

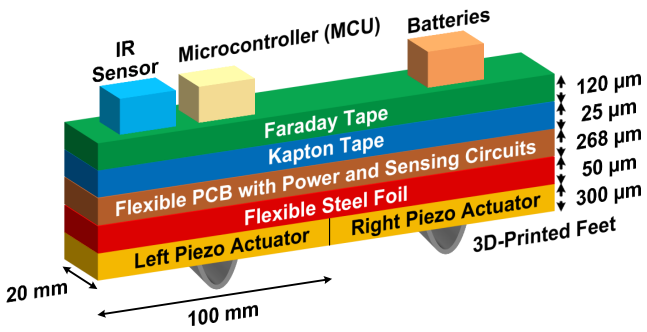

Fig. 2. The mechanical structure of the prototype soft robot. The multi-layer structure includes actuators, power electronics, sensors, control, and energy storage. The sensors detect the speed of the robot. The Kapton and Faraday tapes provide high-voltage insulation and EMI protection. The dimension of an actuator is 100 $\times$ 20 $\times$ 0.3 mm. The steel foil and the PCB are wider than the actuator ($\sim$30 mm).

Figure 1 illustrates the basic operation of a piezoelectric actuator. The piezoelectric actuators used in this work are M-8514-P2 Macro Fiber Composite (MFC) from Smart Material Corp. [15]. They contract when a high voltage is applied across the actuator terminals. The actuators are bonded to a steel foil, which has a higher Young's modulus and tend to retain its length when the actuators contract. Therefore, the steel-bonded actuators bend concave down when a positive voltage is applied. Figure 2 shows the mechanical structure of an example soft robot. The robot is fully-untethered with on-board actuator, power electronics, energy storage, sensing, and wireless communication. Different functions are implemented on different layers for scalable construction and testing.

This work presents a flexible lightweight hybrid switched-capacitor-transformer power converter that can generate a pulsed 300 V to 1500 V, 1 W output from 7.4 V battery voltage with less than 5 g of power electronics. The output of the power converter can be selected among five options:

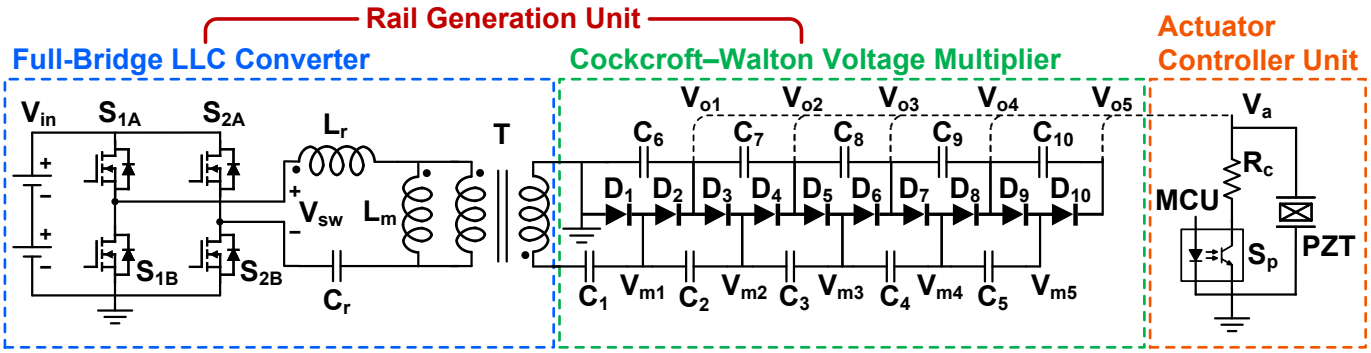

Fig. 3. Schematic of the proposed architecture with a rail generation unit (RGU) and an actuator controller unit (ACU). An RGU comprises an LLC converter and a Cockcroft-Walton voltage multiplier. With a fixed input voltage (V_{in}), the full-bridge LLC topology can adjust the output voltage by frequency modulation or by phase-shifting the two branches of the full-bridge switches. The voltage multiplier offers five outputs with different voltage levels. The input of the ACU (V_a) can be connected to an arbitrary output of the multiplier (V_{o1} to V_{o5}) depending on the need of the actuator.

{300 V, 600 V, 900 V, 1200 V, 1500 V} with voltage regulation enabled by phase-shift control. It can drive the actuators up to 40 Hz with up to 90% dc-to-300 V efficiency.

II. Hybrid Switched-Capacitor-Transformer Power Converter

Figure 3 shows the schematic of the power architecture, comprising two functional modules: the rail generation unit (RGU) and the actuator controller unit (ACU). The RGU generates many linearly scaled voltage rails (e.g., 300 V, 600 V, 900 V, 1200 V, 1500 V in this work), and the ACU controls the ON-OFF operation of the actuator. An onboard microcontroller (MCU) controls the switches in the RGU and ACU. When the MCU enables the full-bridge circuit and turns off S_p, the RGU charges the actuator; when the MCU deactivates the full-bridge switches and turns on S_p, the ACU discharges the load. A set of RGU and ACU together controls an actuator.

The rail generation unit in this work consists of a full-bridge LLC converter and a half-wave Cockcroft-Walton voltage multiplier. A transformer-based voltage converter can offer a high voltage conversion ratio with only low-voltage active switches. The overall voltage gain of the LLC converter can be adjusted by frequency modulation or phase-shifting of the two half-bridges. Figure 4 explains the concept of phase-shift modulation of a full-bridge power converter. The effective input voltage to the resonant tank (V_{SW}) decreases after phase-shifting the two branches of the full-bridge, so the system output voltage can be modulated across a wide range. Switched-capacitor rectifiers are highly modular and can provide high voltage gain. Each stage of the half-wave Cockcroft-Walton voltage multiplier comprises only two capacitors and two diodes and is highly area- and weight-efficient. Each DC output of the voltage multiplier (V_{o1} to V_{o5}) can function as the input of the actuator controller unit based on the required driving voltage of the load actuator, as shown in Fig. 3. If higher driving power is required for the actuators, several rail generation units can be connected in parallel to merge the power. The Cockcroft-Walton rectifier can be further scaled to reach higher voltage levels or provide multiple outputs.

Piezoelectric actuators (PZT in Fig. 3) can be modeled as an RLC network [16], [17], and can be considered as a capacitive

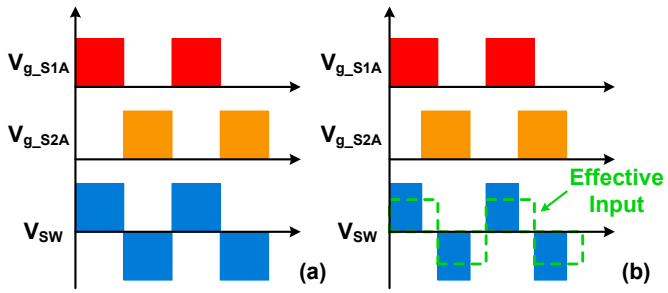

Fig. 4. (a) Non-phase-shifted full-bridge operation. (b) Phase-shifted full-bridge operation. In (b), the waveform of V_{S2A} is phase shifted. The input voltage to the resonant tank (V_{SW}) is 0 V when both V_{S1A} and V_{S2A} are on or off. Therefore, the effective input voltage to the resonant tank reduced, and the output voltage of the system can be modulated. The waveforms of V_{S1B} and V_{S2B} are always out-of-phase with V_{S1A} and V_{S2A}, respectively, to prevent short circuits from input to electrical ground.

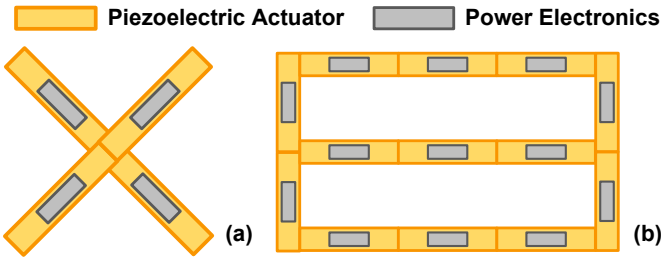

Fig. 5. The scalability and modularity of the proposed power architecture. It can accommodate more complicated multi-actuator arrangements.

load. A current-limiting resistor (R_c in Fig. 3) is included to limit the current charging and discharging the actuator through the MOSFET. S_p is implemented as a ground-referenced MOSFET. To avoid driving the S_p with an additional voltage rail, one may consider using an optically-triggered MOSFET (also known as a solid-state relay or MOSFET relay) to save PCB area and weight budget, with the trade-off of a lower switching speed and current rating. The proposed architecture is modular and scalable. For a multi-actuator soft robot with arbitrary actuator arrangement, multiple sets of RGUs and ACUs can be installed onboard to control different actuators, as shown in Fig. 5. Each set of power electronics can be

TABLE I
BILL-OF-MATERIAL OF THE PROTOTYPE

Component	Description	Each Weight
$S_{1A}-S_{2B}$	24 V BQ500101DPCR	0.05 g
L_r	1.1 μH XEL3520-112MEB	0.11 g
C_r	1206 50 V 1 μF	0.03 g
T	1:20 LPR6235-253PMRC	0.48 g
C_1-C_{10}	1206 450 V 0.1 μF	0.03 g
D_1-D_{10}	350 V BAV5004WS-7	0.02 g
R_c	2512 47 kΩ	0.04 g
S_p	350 V CPC1035N	0.07 g
PZT (P2 MFC)	84 nF M8514-P2	2.30 g

controlled independently, therefore, the array of actuators can be excited with different frequencies, phases, and duty ratios. One can also use one RGU to drive multiple ACUs, or pair an RGU and an ACU as a group for one actuator.

III. PROTOTYPE DESIGN AND EXPERIMENTS

Table I presents the bill-of-material of the soft robot prototype and the weight of each component. Figure 6(a) shows the power converter implemented on a flexible PCB. This flexible PCB contains two piezoelectric actuators with two sets of RGUs and ACUs placed on the left and right sides of the robot. Two 3.7 V lithium polymer batteries are located on the right side of the robot. Figure 6(b) is the enlarged image of a set of RGU and ACU. The complete soft robot prototype is shown in Fig. 6(c), including actuators, power and sensing electronics, microcontroller, batteries, and Kapton and Faraday tapes for EMI shielding.

Figure 7 illustrates the weight distribution of the soft robot across the length of the prototype. Batteries and microcontrollers dominate the weight. They have a significant impact on the locomotion.

Figure 8(a) depicts how each electric component contributes to the total area of the PCB, and Figure 8(b) illustrates how the weight of the entire soft robot is distributed across different function blocks/layers. For each RGU, the LLC converter (including peripheral drivers and control ICs) occupies 636 mm^2 of PCB area and weighs 1.88 g. The specifications for the Cockcroft-Walton voltage multiplier are 92 mm^2 and 0.28 g, and 340 mm^2 and 0.45 g for the actuator controller unit. The total PCB area is 4800 mm^2, and the weight of the whole robot (including the batteries) is 44.5 g.

The prototype design can reliably generate 300 V to 1500 V to drive M-8514-P1 and M-8514-P2 Macro Fiber Composite (MFC) piezoelectric actuators, as reported in [18], [19]. The two-actuator soft robot demonstrated in this work uses M-8514-P2 (300 V) for both actuators. Two 3.7 V 300 mAh lithium polymer batteries (30 $\times$ 20 $\times$ 6 mm, 6.2 g each) are connected in series to provide the 7.4 V input voltage. The full-bridge LLC converter boosts the voltage to 300 V AC, and the Cockcroft-Walton voltage multiplier rectifies the voltage to 300 V DC before multiplication. The voltage conversion ratio of the transformer is 1:20. The full-bridge front end and half-wave back end offer another 2X voltage gain. The overall

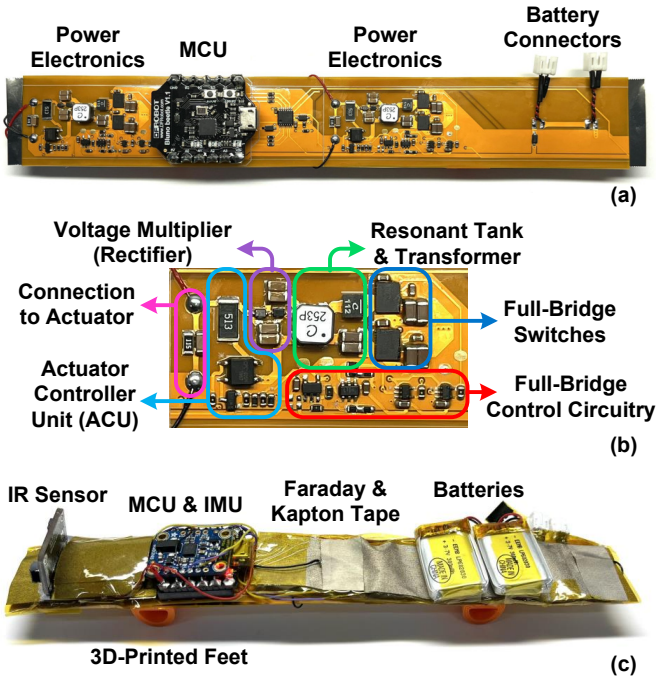

Fig. 6. (a) The circuit prototype of the proposed power architecture. We implemented two sets of RGU and ACU onboard to drive a two-actuator robot. (b) Enlarged photo of a set of RGU and ACU with each function block labelled. (c) The complete robot prototype with actuators, batteries, microcontroller, sensors, power electronics, and Faraday/Kapton tape.

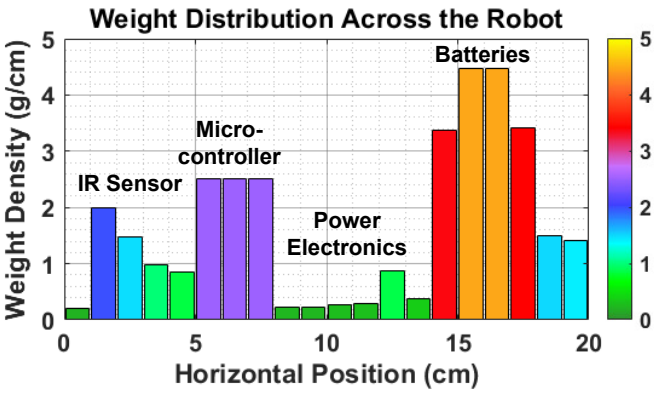

Fig. 7. The weight distribution of components on top of the robot. The weight asymmetry across the length of the prototype contributes to the robot's dynamic locomotion pattern.

voltage gain of the LLC stage before the scalable Cockcroft-Walton voltage multiplier is ~40X (7.4 V to 300 V). This power architecture is capable of supporting actuators with higher voltage levels by extending the stages of the multiplier.

Figure 9 shows the measured waveforms of the prototype in a periodic steady state. At the input side, the full-bridge switches invert the 7.4 V DC input voltage to a square wave with a peak-to-peak value of 14.8 V. At the output side, the rectifier outputs 300 V DC. Figure 10 shows the output waveform when we actively drive a piezoelectric actuator. Ideally, we want to drive an actuator with a high-voltage square wave. In experiments, however, the waveform has slow transition due to the finite charging and discharging time of the power electronics. The ramp-up time and ramp-down time

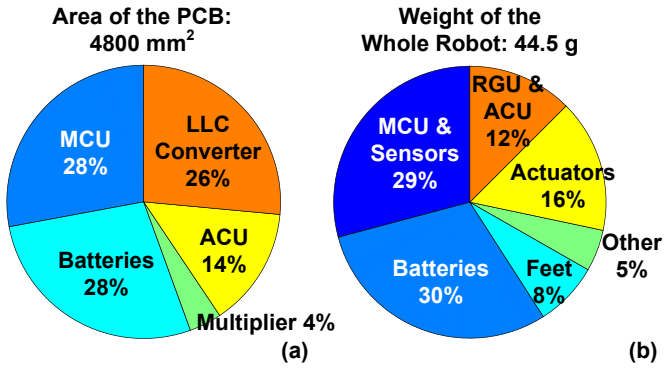

Fig. 8. (a) Pie chart of the PCB area distribution across several function blocks. (b) Pie chart of the weight contribution of each functional block/layer on the complete robot. Energy storage (batteries) consumes the largest area and weight budget.

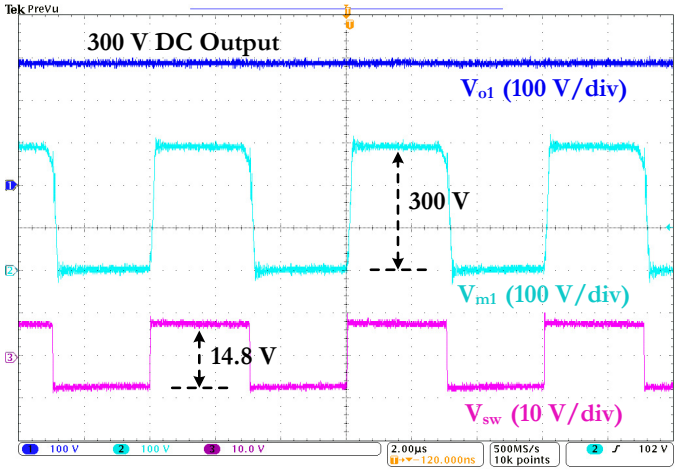

Fig. 9. Waveforms of the circuit prototype. V_{o1} is the 300 V DC output voltage. V_{m1} is the oscillating voltage node of the voltage multiplier. V_{sw} is the input voltage to the LLC resonant tank. The input voltage to the full-bridge switches (V_{in}) is 7.4 V, and the switching frequency is 166 kHz.

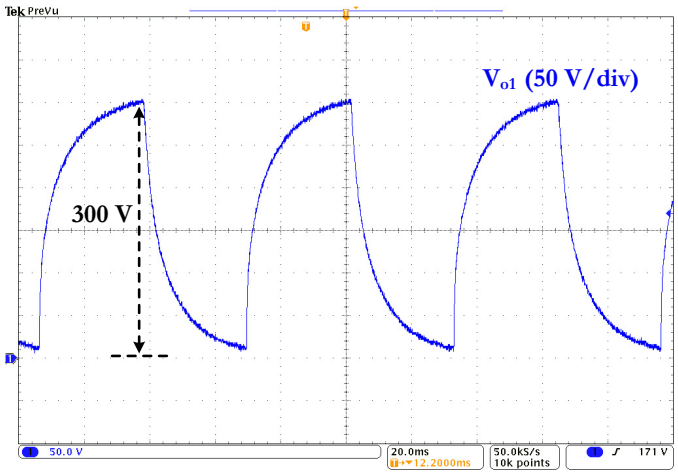

Fig. 10. Waveform of the output voltage when driving a PZT actuator at 16 Hz. Ideally, V_{o1} should be a square wave. Due to the limited current capability of the MOSFETs, the ramp up/down rate of the waveform is reduced.

are both ∼30 ms. The time scale is very different between Fig. 9 and Fig. 10 since the switching frequency of power

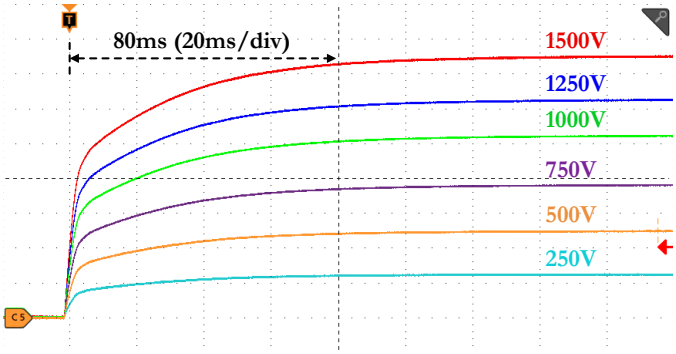

Fig. 11. The start-up transient of generating multiple voltage rails (up to 1500 V) simultaneously. The ramp-up time is ∼80 ms. In this experiment, the basic voltage rail was regulated to 250 V, and the Cockcroft-Walton voltage multiplier has six voltage levels.

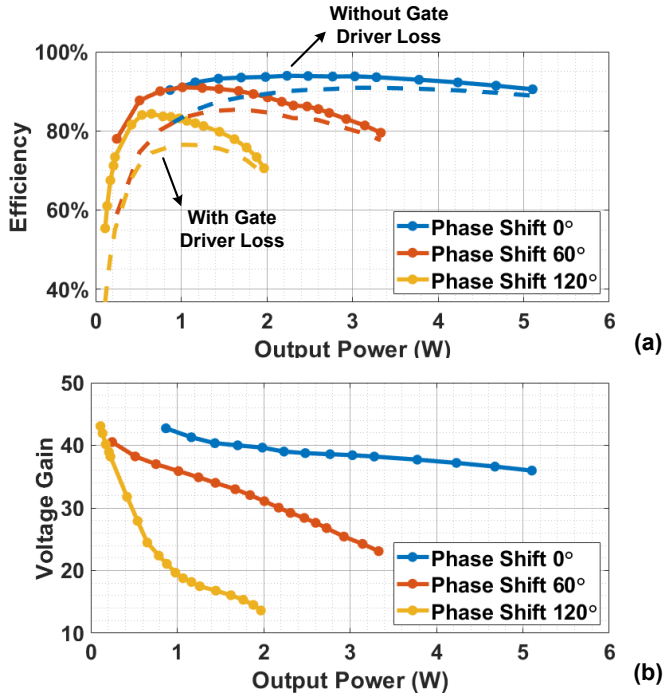

Fig. 12. Efficiency and voltage gain of the RGU with respect to the output power. The legend indicates the phase shift applied to the two half-bridge branches of the full-bridge inverter, and 0° phase shift corresponds to the traditional full-bridge operation. In (a), the solid lines represent the data without considering gate driver loss, and the dashed lines show the estimated efficiencies including gate driver loss.

electronics is many orders higher than the operating frequency of actuators. Figure 11 demonstrates the start-up transient of multiple voltage rails in our previous work [18]. The input voltage is 6.3 V and a six-level Cockcroft-Walton voltage multiplier is used to generate voltage rails up to 1500 V.

The voltage gain of the circuit can be modulated by phase-shifting the two half-bridge branches of the full-bridge inverter, at the expense of lower efficiency at a larger phase shift. Figure 12 shows the efficiency and voltage gain measured at different phase shifts. After considering gate driver loss, the rail generation unit's peak efficiency is 90.9% at 0° phase shift and 76.5% at 120° phase shift. The phase shift modulation presents another degree of freedom for modulating the voltage gain of a full-bridge LLC converter other than frequency

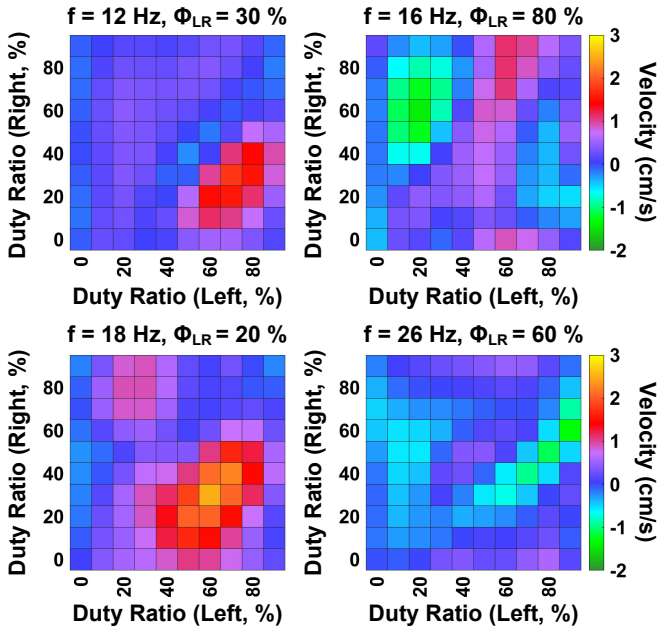

Fig. 13. Velocity of the soft robot at various operating conditions. In each graph, the data is plotted with respect to the duty ratios of the left and right actuators at a fixed frequency and phase. The color bar depicts the velocity.

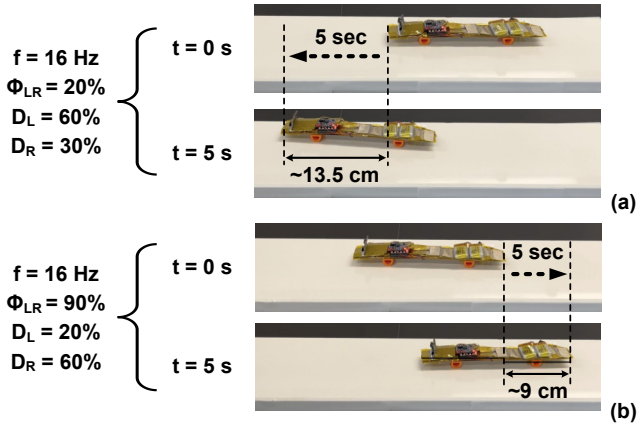

Fig. 14. The prototype soft robot can move left at 2.7 cm/s and move right at 1.8 cm/s when driven at different operation points. The robot is operated for 5 seconds for velocity calculation.

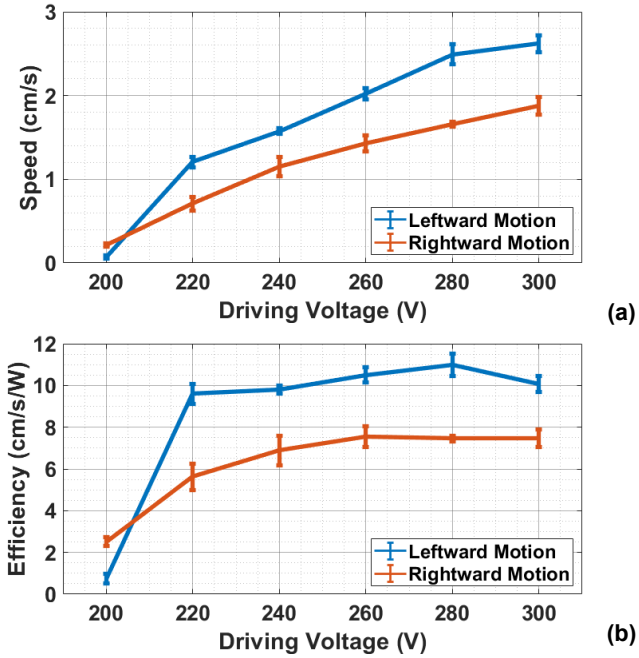

Fig. 15. (a) Absolute velocity (speed) and (b) locomotion efficiency with respect to the driving voltage. The robot's speed has a monotonic relation with the voltage applied to actuators. However, the locomotion efficiency does not keep rising with increasing driving voltage. The operation points of the leftward and rightward motion are the same as Fig. 14.

modulation, making a full-bridge design more attractive than half-bridge options.

The robot prototype is capable of untethered operation, and each power module on the robot can be controlled independently. We apply high-voltage square waves to each actuator at different frequencies, phases (related to other actuators), and duty ratios and measure the velocity of the robot. At each operation point, we drive the robot for 5 seconds, then the microcontroller records the information obtained from the onboard distance sensor. After that, the MCU transmits the data back to a PC via Bluetooth. The prototype soft robot exhibits various locomotion velocities at different operation points, as shown in Figure 13. The reason for the dynamic behavior is related to the actuation pattern (frequency, phase, duty ratio) and the weight distribution across the length of the robot. The maximum speed of the soft robot is 2.7 cm/s for moving left and 1.8 cm/s for moving right. Figure 14 contains the video screenshots of these two operating conditions. In Figures 13 and 14, f is the operating frequency, Φ_{LR} denotes the phase, D_L and D_R represent the duty ratio of the left and right actuator. Detailed simulation and experiments on locomotion and energy efficiency are presented in [20]–[23].

The actuators are driven at 300 V in all experimental results above. However, it is also interesting to investigate the robot behavior at a lower driving voltage. The results are shown in Figure 15, and the operation points of the leftward and rightward motion are the same as Figure 14. The absolute velocity (speed) monotonically decreases with decreasing driving voltage. The locomotion efficiency can be calculated by dividing the speed by power consumption of the power circuitry. The efficiency for the leftward motion at 280 V is $\sim$10% higher than the value at 300 V. For the rightward motion, the efficiencies are almost the same between 260 V and 300 V. This information indicates that the actuators can be driven at higher voltage if higher speed is desired. However, if efficiency is the main concern (for longer run time or battery power preservation), then slightly decreasing the driving voltage could be a viable option. More experiments can be done to verify the voltage-efficiency behavior of the soft robot and to jointly optimize the locomotion efficiency and the cost of transportation.

The curvature of soft actuators can influence a soft robot's locomotion speed, efficiency, and ability to conform to the environment. A closed-loop sensing-control strategy is needed to further optimize the driving voltage and the actuator curvature of the soft robot. We leverage strain sensors to measure the curvature of a piezoelectric actuator. Figure 16 shows the

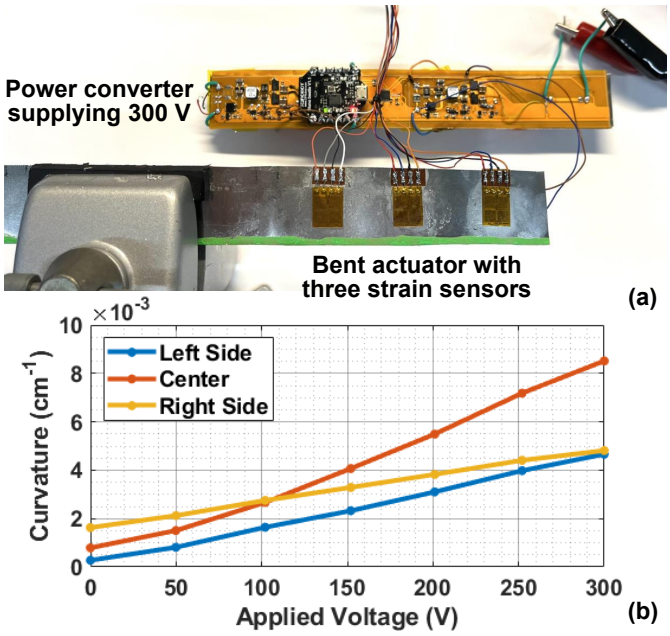

Fig. 16. (a) Experimental setup of the curvature measurement. Three strain sensors are installed on the steel foil of an actuator. The measured curvature is 4.7×10^{-3}, 8.5×10^{-3}, 4.8×10^{-3} cm^{-1} at the left side, center, and right side when 300 V is applied to the actuator. (b) The measured curvature with various applied voltages. The center part of the actuator usually has larger curvature than the left and right parts.

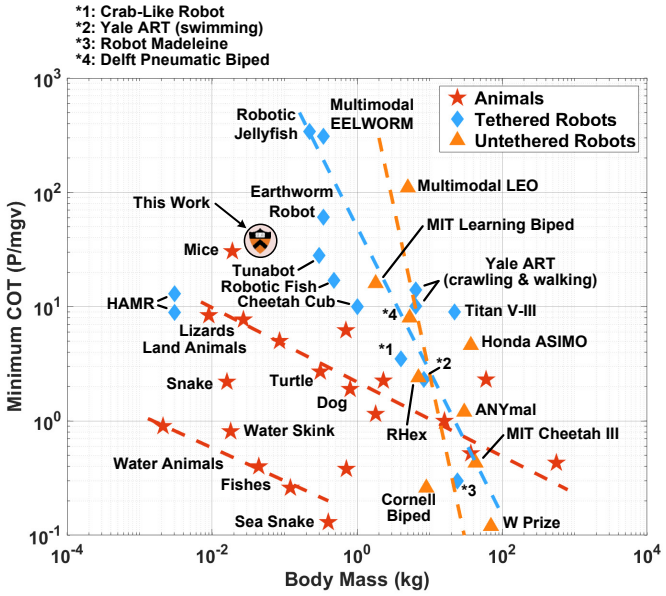

Fig. 17. The cost of transport of various animals, tethered robots, untethered robots, and the prototype in this work. Data recreated from [24].

experimental setup and measured data. The results show that a bent actuator does not represent a perfect arc of a circle. Instead, it usually has higher curvature in the middle and lower curvature on both sides, motivating more advanced modeling, control, and multi-disciplinary co-optimization.

Cost of transport (COT) is a figure-of-merit (FOM) that is commonly used to compare the locomotion efficiency across robotic systems [24]. COT $= \frac{P}{mgv}$. It considers the power consumption (P) in the unit of Watt, mass (m) in the unit of kg, acceleration due to gravity (g) in the unit of m/s^2, and the speed (v) of the robot in the unit of m/s [24]. For our two-actuator prototype, $P = 0.46$ W, $m = 0.0445$ kg, $g = 9.8$ m/s^2, $v = 0.027$ m/s, and the COT is about 39.1 W/(kg·m^2/s^3). As shown in Fig. 17, the weight of the prototype is lower than most other robotic systems, and the cost of transport is comparable to mice. The data in Fig. 17 are recreated from [24]. The COTs for animals and robotic systems are obtained from [24]–[43].

IV. Conclusion

This paper presents a scalable, lightweight, high voltage conversion ratio hybrid switched-capacitor-transformer power architecture for untethered multi-actuator piezoelectric soft robots. The dc-dc converter is able to generate 300 V to 1500 V from 7.4 V with a peak efficiency higher than 90%. The weight of the power converter is less than 5 g. The circuit can be reconfigured to drive many actuators. The voltage gain of the LLC converter is adjustable. The stage count of the voltage multiplier is scalable. The proposed power architecture is widely applicable to driving an array of macro fiber composite (MFC) piezoelectric actuators in soft robots with different voltages, frequencies, phases, and duty ratios while maintaining high efficiency, high power density, and compact size.

A fully untethered soft robot enables systematic hardware, software, control, and power co-design. We see soft robots and power electronics co-design opportunities in the following three aspects:

- Electrical-Power Co-Design: The electrical behaviors of soft robotic actuators are usually frequency-, amplitude-, and waveform-dependent. Power electronics that can generate desired actuation waveforms while maintain high electrical efficiency are desired to optimize the overall system electrical efficiency.
- Mechanical-Power Co-Design: Structural design and weight distribution can significantly influence the mechanical dynamics of soft robots. Co-packaging, shielding, and insulation of power electronics need to be jointly considered with the design of the soft robots.
- Control-Power Co-Design: The control of the power electronics and the control of the soft robots are jointly related. The high-efficiency operation regions of power electronics may not overlap with the high-efficiency control patterns of the soft robots.

References

[1] Y. Wu, J. K. Yim, J. Liang, Z. Shao, M. Qi, J. Zhong, Z. Luo, X. Yan, M. Zhang, X. Wang, R. S. Fearing, R. J. Full, and L. Lin, "Insect-scale fast moving and ultrarobust soft robot," *Science Robotics*, vol. 4, no. 32, 2019. [Online]. Available: https://robotics.sciencemag.org/content/4/32/eaax1594

[2] K. Y. Ma, P. Chirarattananon, S. B. Fuller, and R. J. Wood, "Controlled flight of a biologically inspired, insect-scale robot," *Science*, vol. 340, no. 6132, pp. 603–607, 2013. [Online]. Available: https://science.sciencemag.org/content/340/6132/603

[3] Y. Wu, K. Y. Ho, K. Kariya, R. Xu, W. Cai, J. Zhong, Y. Ma, M. Zhang, X. Wang, and L. Lin, "Pre-curved PVDF/PI unimorph structures for biomimic soft crawling actuators," in *2018 IEEE Micro Electro Mechanical Systems (MEMS)*, 2018, pp. 581–584.

[4] P. Xiao, N. Yi, T. Zhang, Y. Huang, H. Chang, Y. Yang, Y. Zhou, and Y. Chen, "Construction of a fish-like robot based on high performance graphene/PVDF bimorph actuation materials," *Advanced Science*, vol. 3, no. 6, p. 1500438, 2016. [Online]. Available: https://onlinelibrary.wiley.com/doi/abs/10.1002/advs.201500438

[5] S. Mohith, A. R. Upadhya, N. Karanth, S. Kulkarni, and M. Rao, "Recent trends in piezoelectric actuators for precision motion and their applications: A review," *Smart Materials and Structures*, 2020.

[6] S. Park, D. S. Drew, S. Follmer, and J. Rivas-Davila, "Lightweight high voltage generator for untethered electroadhesive perching of micro air vehicles," *IEEE Robotics and Automation Letters*, vol. 5, no. 3, pp. 4485–4492, 2020.

[7] H. Xu, Y. He, K. L. Strobel, C. K. Gilmore, S. P. Kelley, C. C. Hennick, T. Sebastian, M. R. Woolston, D. J. Perreault, and S. R. H. Barrett, "Flight of an aeroplane with solid-state propulsion," *Nature*, vol. 563, p. 532–535, 2018.

[8] G. Li, X. Chen, F. Zhou, Y. Liang, Y. Xiao, X. Cao, Z. Zhang, M. Zhang, B. Wu, S. Yin, Y. Xu, H. Fan, Z. Chen, W. Song, W. Yang, B. Pan, J. Hou, W. Zou, S. He, X. Yang, G. Mao, Z. Jia, H. Zhou, T. Li, S. Qu, Z. Xu, Z. Huang, Y. Luo, T. Xie, J. Gu, S. Zhu, and W. Yang, "Self-powered soft robot in the mariana trench," *Nature*, vol. 591, p. 66–71, 2020.

[9] Y. He, M. Woolston, and D. Perreault, "Design and implementation of a lightweight high-voltage power converter for electro-aerodynamic propulsion," in *2017 IEEE 18th Workshop on Control and Modeling for Power Electronics (COMPEL)*, 2017, pp. 1–9.

[10] T. Xie, M. R. Oltra, and H.-P. Le, "A 5kV/15W dual-transformer hybrid converter with extreme 2000X conversion ratios for soft mobile robots," in *2020 IEEE Applied Power Electronics Conference and Exposition (APEC)*, 2020, pp. 1548–1552.

[11] J. Liang, Y. Wu, J. K. Yim, H. Chen, Z. Miao, H. Liu, Y. Liu, Y. Liu, D. Wang, W. Qiu *et al.*, "Electrostatic footpads enable agile insect-scale soft robots with trajectory control," *Science Robotics*, vol. 6, no. 55, p. eabe7906, 2021.

[12] V. A. K. Prabhala, P. Fajri, V. S. P. Gouribhatla, B. P. Baddipadiga, and M. Ferdowsi, "A DC–DC converter with high voltage gain and two input boost stages," *IEEE Transactions on Power Electronics*, vol. 31, no. 6, pp. 4206–4215, 2015.

[13] Y. Li, B. L. Dobbins, and J. T. Stauth, "33.8 A decentralized daisy-chain-controlled switched-capacitor driver for microrobotic actuators with $10\times$ power-reduction factor and over 300V drive voltage," in *2021 IEEE International Solid-State Circuits Conference (ISSCC)*, vol. 64. IEEE, 2021, pp. 474–476.

[14] Y. Li, B. Mabetha, and J. T. Stauth, "A 3.7V-to-1kV chip-cascaded switched-capacitor converter with auxiliary boost achieving $> 96\%$ reactive power efficiency for electrostatic drive applications," in *2023 IEEE International Solid-State Circuits Conference (ISSCC)*, 2023.

[15] "Smart Material Corp. Sarasota, Florida. Part number: M-8514-P2." [Online]. Available: https://www.smart-material.com/media/Datasheets/MFC_V2.4-datasheet-web.pdf

[16] M. Karpelson, G.-Y. Wei, and R. J. Wood, "Driving high voltage piezoelectric actuators in microrobotic applications," *Sensors and Actuators A: Physical*, vol. 176, pp. 78–89, 2012. [Online]. Available: https://www.sciencedirect.com/science/article/pii/S0924424711006947

[17] S. Sherrit, H. Wiederick, and B. Mukherjee, "Accurate equivalent circuits for unloaded piezoelectric resonators," in *1997 IEEE Ultrasonics Symposium Proceedings. An International Symposium (Cat. No.97CH36118)*, vol. 2, 1997, pp. 931–935.

[18] H. Cheng, Z. Zheng, P. Kumar, Y. Chen, and M. Chen, "Hybrid-SoRo: Hybrid switched capacitor power management architecture for multi-channel piezoelectric soft robot," in *2022 IEEE Applied Power Electronics Conference and Exposition (APEC)*, 2022, pp. 1338–1344.

[19] Z. Zheng, H. Cheng, P. Kumar, S. Wagner, M. Chen, N. Verma, and J. C. Sturm, "Wirelessly-controlled untethered piezoelectric planar soft robot capable of bidirectional crawling and rotation," *2023 IEEE International Conference on Robotics and Automation (ICRA)*, 2023.

[20] Z. Zheng, P. Kumar, Y. Chen, H. Cheng, S. Wagner, M. Chen, N. Verma, and J. C. Sturm, "Piezoelectric soft robot inchworm motion by controlling ground friction through robot shape," *arXiv preprint arXiv:2111.00944*, 2021.

[21] Z. Zheng, P. Kumar, Y. Chen, H. Cheng, S. Wagner, M. Chen, N. Verma, and J. C. Sturm, "Model-based control of planar piezoelectric inchworm soft robot for crawling in constrained environments," in *2022 IEEE 5th Inter. Conf. on Soft Robo. (RoboSoft)*, 2022.

[22] Z. Zheng, P. Kumar, Y. Chen, H. Cheng, S. Wagner, M. Chen, N. Verma, and J. C. Sturm, "Scalable simulation and demonstration of jumping piezoelectric 2-d soft robots," in *2022 International Conference on Robotics and Automation (ICRA)*, 2022, pp. 5199–5204.

[23] H. Cheng, Z. Zheng, P. Kumar, W. Afridi, B. Kim, S. Wagner, N. Verma, J. C. Sturm, and M. Chen, "eViper: A scalable platform for untethered modular soft robots," *2023 IEEE/RSJ International Conference on Intelligent Robots and Systems (IROS 2023)*, 2023.

[24] R. Baines, S. K. Patiballa, J. Booth, L. Ramirez, T. Sipple, A. Garcia, F. Fish, and R. Kramer-Bottiglio, "Multi-environment robotic transitions through adaptive morphogenesis," *Nature*, vol. 610, no. 7931, pp. 283–289, Oct 2022. [Online]. Available: https://doi.org/10.1038/s41586-022-05188-w

[25] E. Milana, B. V. Raemdonck, K. Cornelis, E. Dehaerne, J. D. Clerck, Y. D. Groof, T. D. Vil, B. Gorissen, and D. Reynaerts, "EELWORM: a bioinspired multimodal amphibious soft robot," in *2020 3rd IEEE International Conference on Soft Robotics (RoboSoft)*, 2020, pp. 766–771.

[26] S. Kitano, S. Hirose, A. Horigome, and G. Endo, "TITAN-XIII: sprawling-type quadruped robot with ability of fast and energy-efficient walking," *Robomech Journal*, vol. 3, pp. 1–16, 2016.

[27] A. Kandhari, Y. Wang, H. J. Chiel, R. D. Quinn, and K. A. Daltorio, "An analysis of peristaltic locomotion for maximizing velocity or minimizing cost of transport of earthworm-like robots," *Soft Robotics*, vol. 8, no. 4, pp. 485–505, 2021.

[28] K. Kim, P. Spieler, E.-S. Lupu, A. Ramezani, and S.-J. Chung, "A bipedal walking robot that can fly, slackline, and skateboard," *Science Robotics*, vol. 6, no. 59, p. eabf8136, 2021.

[29] G. Bledt, M. J. Powell, B. Katz, J. Di Carlo, P. M. Wensing, and S. Kim, "MIT Cheetah 3: Design and control of a robust, dynamic quadruped robot," in *2018 IEEE/RSJ International Conference on Intelligent Robots and Systems (IROS)*, 2018, pp. 2245–2252.

[30] M. Hutter, C. Gehring, D. Jud, A. Lauber, C. D. Bellicoso, V. Tsounis, J. Hwangbo, K. Bodie, P. Fankhauser, M. Bloesch, R. Diethelm, S. Bachmann, A. Melzer, and M. Hoepflinger, "ANYmal - a highly mobile and dynamic quadrupedal robot," in *2016 IEEE/RSJ International Conference on Intelligent Robots and Systems (IROS)*, 2016, pp. 38–44.

[31] G. Wang, X. Chen, S. Yang, P. Jia, X. Yan, and J. Xie, "Subsea crab bounding gait of leg-paddle hybrid driven shoal crablike robot," *Mechatronics*, vol. 48, pp. 1–11, 2017.

[32] J. H. Long, J. Schumacher, N. Livingston, and M. Kemp, "Four flippers or two? Tetrapodal swimming with an aquatic robot," *Bioinspiration & Biomimetics*, vol. 1, no. 1, p. 20, 2006.

[33] M. Wisse, G. Feliksdal, J. V. Frankenhuyzen, and B. Moyer, "Passive-based walking robot," *IEEE Robotics & Automation Magazine*, vol. 14, no. 2, pp. 52–62, 2007.

[34] Y. Sakagami, R. Watanabe, C. Aoyama, S. Matsunaga, N. Higaki, and K. Fujimura, "The intelligent ASIMO: System overview and integration," in *IEEE/RSJ international conference on intelligent robots and systems*, vol. 3. IEEE, 2002, pp. 2478–2483.

[35] S. Collins, A. Ruina, R. Tedrake, and M. Wisse, "Efficient bipedal robots based on passive-dynamic walkers," *Science*, vol. 307, no. 5712, pp. 1082–1085, 2005.

[36] A. Kuo, "Choosing your steps carefully," *IEEE Robotics & Automation Magazine*, vol. 14, no. 2, pp. 18–29, 2007.

[37] C. H. White, G. V. Lauder, and H. Bart-Smith, "Tunabot Flex: A tuna-inspired robot with body flexibility improves high-performance swimming," *Bioinspiration & Biomimetics*, vol. 16, no. 2, 2021.

[38] V. A. Tucker *et al.*, "Energetic cost of locomotion in animals." *Comparative Biochemistry and Physiology*, vol. 34, pp. 841–846, 1970.

[39] Y. Chen, N. Doshi, B. Goldberg, H. Wang, and R. J. Wood, "Controllable water surface to underwater transition through electrowetting in a hybrid terrestrial-aquatic microrobot," *Nature communications*, vol. 9, no. 1, p. 2495, 2018.

[40] W. I. Sellers, K. A. Rose, D. A. Crossley II, and J. R. Codd, "Inferring cost of transport from whole-body kinematics in three sympatric turtle species with different locomotor habits," *Comparative Biochemistry and Physiology Part A: Molecular & Integrative Physiology*, vol. 247, p. 110739, 2020.

[41] F. Berlinger, M. Saadat, H. Haj-Hariri, G. Lauder, and R. Nagpal, "Fish-like three-dimensional swimming with an autonomous, multi-fin, and biomimetic robot," *Bioinspiration & Biomimetics*, vol. 16, no. 2, p. 026018, 2021.

[42] N. Kau, A. Schultz, N. Ferrante, and P. Slade, "Stanford Doggo: An open-source, quasi-direct-drive quadruped," in *2019 International Conference on Robotics and Automation (ICRA)*, 2019, pp. 6309–6315.

[43] U. Saranli, M. Buehler, and D. E. Koditschek, "RHex: A simple and highly mobile hexapod robot," *The International Journal of Robotics Research*, vol. 20, no. 7, pp. 616–631, 2001.